Global Biogeochemical Cycles®

RESEARCH ARTICLE
10.1029/2022GB007617

Influence of Changes in pH and Temperature on the Distribution of Apparent Iron Solubility in the Oceans

Kechen Zhu[1,2], Eric P. Achterberg[1], Nicholas R. Bates[3,4], Loes J. A. Gerringa[5], Rob Middag[5,6], Mark J. Hopwood[7], and Martha Gledhill[1]

[1]GEOMAR Helmholtz Center for Ocean Research Kiel, Kiel, Germany, [2]Now at Southern University of Science and Technology, Shenzhen, China, [3]Bermuda Institute of Ocean Science, St. George's, Bermuda, [4]Department of Ocean and Earth Science, National Oceanography Center, University of Southampton, Southampton, UK, [5]Department of Ocean Systems, NIOZ, Royal Netherlands Institute for Sea Research, Texel, The Netherlands, [6]Department of Geology and Centre for Trace Element Analysis, University of Otago, Dunedin, New Zealand, [7]Department of Ocean Science and Engineering, Southern University of Science and Technology, Shenzhen, China

Key Points:

- Apparent iron solubility is driven by ambient pH, temperature (T) and dissolved organic carbon (DOC) and showed a 6-fold variation between surface (pH = 8.05 on the total scale, DOC = 71.8 μmol L^{-1}, T = 20.4°C) and deep oceanic waters (pH = 7.82, DOC = 38.6 μmol L^{-1}, T = 1.1°C)
- Higher values of apparent iron solubility were determined for deep Atlantic and Pacific waters, with lower values in subtropical gyres
- Calculated apparent iron solubility showed a similar trend in vertical distribution to dissolved iron, highlighting the importance of considering the impact of changes in ambient physico-chemical conditions on seawater iron chemistry

Supporting Information:

Supporting Information may be found in the online version of this article.

Correspondence to:

K. Zhu,
zhukechen@cau.edu.cn

Citation:

Zhu, K., Achterberg, E. P., Bates, N. R., Gerringa, L. J. A., Middag, R., Hopwood, M. J., & Gledhill, M. (2023). Influence of changes in pH and temperature on the distribution of apparent iron solubility in the oceans. *Global Biogeochemical Cycles*, *37*, e2022GB007617. https://doi.org/10.1029/2022GB007617

Received 18 OCT 2022
Accepted 1 MAY 2023

Abstract An insufficient supply of the micronutrient iron (Fe) limits phytoplankton growth across large parts of the ocean. Ambient Fe speciation and solubility are largely dependent on seawater physico-chemical properties. We calculated the apparent Fe solubility ($SFe(III)_{app}$) at equilibrium for ambient conditions, where $SFe(III)_{app}$ is defined as the sum of aqueous inorganic Fe(III) species and Fe(III) bound to organic matter formed at a free Fe^{3+} concentration equal to the solubility of Fe hydroxide. We compared the $SFe(III)_{app}$ to measured dissolved Fe (dFe) in the Atlantic and Pacific Oceans. The $SFe(III)_{app}$ was overall ~2–4-fold higher than observed dFe at depths less than 1,000 m, ~2-fold higher than the dFe between 1,000 and 4,000 m and ~3-fold higher than dFe below 4,000 m. Within the range of used parameters, our results showed that there was a similar trend in the vertical distributions of horizontally averaged $SFe(III)_{app}$ and dFe. Our results suggest that vertical dFe distributions are underpinned by changes in $SFe(III)_{app}$, which are driven by relative changes in ambient pH and temperature. Since both pH and temperature are essential parameters controlling ambient Fe speciation, these should be accounted for in investigations of changing Fe dynamics, particularly in the context of ocean acidification and warming.

1. Introduction

Iron (Fe) is an essential micronutrient for a range of biochemical processes and its low availability limits primary productivity in ca. 40% of the world's ocean (Boyd et al., 2007). This is the result of low solubility of the thermodynamically favored Fe(III) species in oxic (dissolved oxygen >2 mg L^{-1}) seawater (Liu & Millero, 2002) as well as the tendency for Fe to be "scavenged" from the water column by sinking particles (Tagliabue et al., 2017). In seawater, dissolved Fe (dFe, operationally defined by filtration, typically at 0.2 μm) is complexed by dissolved organic matter (DOM), which increases Fe solubility and controls Fe(III) speciation (Gledhill & Buck, 2012). Current understanding suggests that there is an overall excess of binding capacity for Fe in seawater, that is, an excess of Fe-binding ligands, and only slight variations in binding characteristics on an ocean basin scale, especially in deep waters (Buck et al., 2015, 2018; Gerringa et al., 2015). It should be noted however that these binding characteristics are typically determined at a single pH (either e.g., 8.05 or 8.2 depending on the method) and at room temperature (ca. 20°C). The relative uniformity of Fe-binding characteristics that are indirectly determined via titrations suggests that the concentrations and characteristics of DOM that binds Fe do not vary greatly over large spatial and temporal scales. Whilst Fe-binding characteristics appear to be relatively uniform in space and time, organic matter itself is highly heterogeneous (Zark & Dittmar, 2018) and cation binding site distributions within marine DOM reflect this heterogeneity (Lodeiro et al., 2020, 2021). Marine DOM thus contains acidic and basic binding groups with variable affinities for H^+ and metal ions (Lodeiro et al., 2021; Zhang et al., 2019), factors which have not generally been accounted for investigations of chemical Fe speciation in seawater.

The capacity of organic matter to bind Fe is not determined by the concentration and affinity of the binding sites alone, but also by changes in ambient physico-chemical conditions such as pH, temperature, dissolved oxygen concentrations (or Eh, electrochemical potentials) and ionic strength. Seawater pH in the present day ocean varies from ca. 8.2 (on the total pH scale) in subpolar and polar surface waters (Takahashi et al., 2014) to ca. 7.6 (on the total pH scale) in eastern boundary upwelling regions (Bates, 2018). Temperatures in surface waters of up to ca.

35°C are observed in the tropics compared to ca. −2°C near the poles. Furthermore, these pH and temperature ranges are not static. The ocean has taken up ca. 30% of emitted anthropogenic CO_2 since the preindustrial era, while atmospheric CO_2 concentrations increased from 280 to 400 ppm, which has resulted in an average 0.1 unit pH decline (from 8.2 to 8.1) in the surface ocean (Garcia-Soto et al., 2021; IPCC, 2013). This decrease in ocean pH is projected to continue and pH could drop by a further 0.33 pH unit by the end of this century under the IPCC RCP8.5 "business-as-usual" scenario (Jiang et al., 2019).

To account for changes in Fe speciation with pH, given a heterogeneous Fe-binding ligand pool (Perdue & Lytle, 1983), intrinsic equilibrium constants that represent binding site heterogeneity are required. Such approaches are provided by, for example, the NICA-Donnan model (Kinniburgh et al., 1999) and WHAM/Model VII (Tipping et al., 2011). These models simulate competition between protons, major cations and metal ions binding to heterogeneous groups of binding sites such as those comprising organic matter in terrestrial and freshwater systems. Both models use two major types of binding sites, carboxylic-type groups (acidity constants, pKa < ca. 6) and phenolic-type groups (acidity constants, pKa > ca. 7) (Perdue, 1985). The NICA-Donnan model assumes binding sites with a continuous range of binding affinity for protons, major ions and metals, whereas the WHAM/Model VII employs four sets of discrete binding sites for each type. Available parameters describing proton and major ion (calcium, magnesium) binding for both models are derived from experimental data of humic substances isolated from freshwater or terrestrial environments. Nevertheless, both the NICA-Donnan model and WHAM/Model VII provide consistent results for Fe solubility, titration experiments and elemental stoichiometry of DOM in seawater (Gledhill et al., 2015, 2022; Hiemstra & Van Riemsdijk, 2006; Stockdale et al., 2015), which suggests that the binding site heterogeneity of marine DOM is likely to be similar to that of terrestrial DOM.

Iron solubility is also known to be directly influenced by temperature and pH (Liu & Millero, 1999). Iron solubility is defined relative to the solubility product ($K^*_{Fe(OH)3}$) of Fe hydroxide ($Fe(OH)_3(s)$) according to Equations 1 and 2

$$Fe^{3+} + 3OH^- \rightarrow Fe(OH)_3(s) \quad (1)$$

$$K^*_{Fe(OH)3} = \frac{[Fe^{3+}]}{(H^+)^3} = -13.486 - 0.1856I^{0.5} + 0.30731I + 5254/T \quad (2)$$

(Liu & Millero, 1999) where I is the ionic strength (molality) and T is the temperature (K). Iron solubility therefore increases with decreasing pH and temperature, although binding to organic matter may have a mitigating effect (Liu & Millero, 2002). Iron binding by DOM influences Fe solubility by modifying the concentration of Fe^{3+} together with the inorganic complexation of OH^- (Equations 3 and 4).

$$Fe^{3+} + DOM \leftrightarrow FeDOM \quad (3)$$

$$Fe^{3+} + 3OH^- \leftrightarrow Fe(OH)_3 \quad (4)$$

Hence, the overall inventory of dFe is dependent on the interaction between Fe solubility and the binding capacity of DOM (Johnson et al., 1997; Kuma et al., 2003; Liu & Millero, 2002). We have derived a parameter, the apparent Fe solubility ($SFe(III)_{app}$), defined as the sum of aqueous inorganic Fe(III) species and Fe(III) bound to DOM formed at a free Fe (Fe^{3+}) concentration equal to the limiting solubility of Fe hydroxide ($Fe(OH)_3(s)$) (Zhu, Birchill, et al., 2021; Zhu, Hopwood, et al., 2021). Apparent Fe solubility can be considered as a chemical approximation of the dFe buffering capacity for ambient seawater conditions. Taking advantage of the first set of proton binding constants for marine DOM that were derived for the brackish Baltic Sea (Lodeiro et al., 2020), Zhu, Hopwood, et al. (2021) derived NICA constants for Fe(III) binding to marine DOM and subsequently calculated speciation and solubility of Fe(III) for the water column of the Peruvian shelf and slope region using an ion pairing-organic matter (NICA-Donnan) model. Results indicated that a decreased pH as a result of intense organic matter remineralization in the oxygen minimum zone and ocean acidification could increase the $SFe(III)_{app}$ and thus potentially facilitate an increased supply of dFe to surface waters, together with other processes for example, reduced Fe(II) species from suboxic sedimentary input.

In this work, we applied these new NICA constants for marine DOM (Lodeiro et al., 2020; Zhu, Hopwood, et al., 2021) to predict the $SFe(III)_{app}$ in the Atlantic and Pacific Oceans at ambient pH, temperature and dissolved organic carbon (DOC) concentrations. We use discrete sample data available in the IDP2021 database

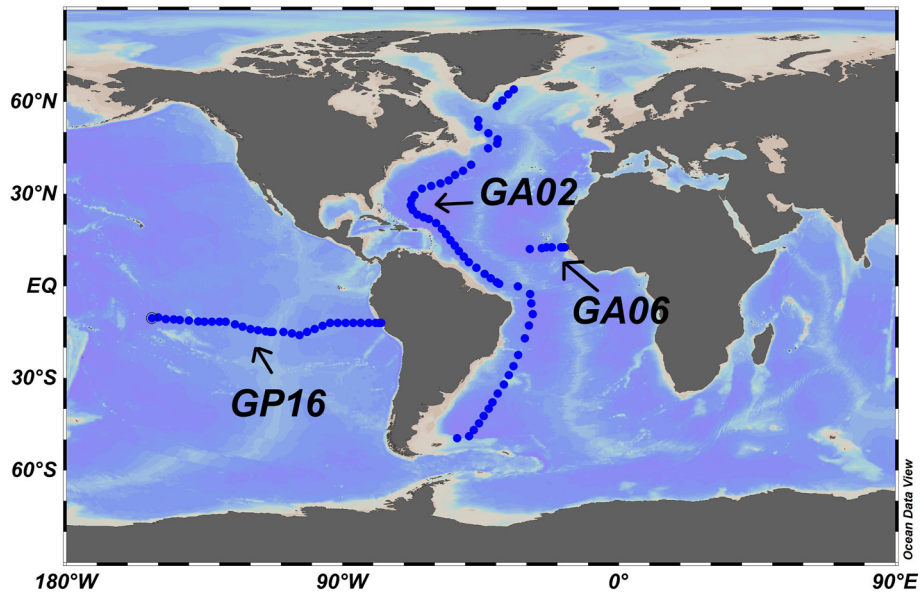

Figure 1. Map of study area along the West Atlantic Ocean transect (GA02, April–July 2010 and March–April 2011), Subtropical North Atlantic Ocean transect (GA06, February–March 2011) and Southeast Pacific Ocean transect (GP16, October–December 2013), generated in Ocean Data View (Schlitzer, 2023).

(GEOTRACES Intermediate Data Product Group, 2021) for pH, DOC and dFe determined from a series of GEOTRACES cruises, along a West Atlantic Ocean transect, Subtropical North Atlantic Ocean transect and Southeast Pacific Ocean transect. The cruises were selected to cover a large part of the pH, dFe and DOC range expected in the Atlantic and Pacific Oceans. We compared the calculated $SFe(III)_{app}$ to measured dFe at basin scales, and then examined the correlations among dFe, $SFe(III)_{app}$, pH, temperature, DOC, salinity and phosphate. Our work aims to assess how changes in ambient conditions, such as pH and temperature, impact predicted $SFe(III)_{app}$ in the water column and to determine the potential implications for the ocean dFe inventory in the context of expected changes in pH and temperature in a more acidic and warmer ocean.

2. Materials and Methods

2.1. Observational Data

Observational data used in this work were collected during a series of GEOTRACES cruises along the whole West Atlantic Ocean (GEOTRACES GA02; April–July 2010 and March–April 2011), Subtropical North Atlantic Ocean (GEOTRACES GA06; February–March 2011) and Southeast Pacific Ocean (GEOTRACES GP16; October–December 2013) (Figure 1). Depth, potential temperature (in the ITS-90 convention) and practical salinity were measured using CTD sensors attached to rosette frames. The pH was calculated from dissolved inorganic carbon (C_T) and total alkalinity (A_T), and DOC and dFe concentrations were obtained from discrete samples. For cruise GA02, results of C_T and A_T, DOC and dFe were directly taken from the GEOTRACES database IDP2021 (GEOTRACES Intermediate Data Product Group, 2021); the GA02 results for C_T and A_T were partially described by Salt et al. (2015). Details of dFe and DOC distributions for GA02 were described by Gerringa et al. (2015) and Rijkenberg et al. (2014). For cruise GP16, the results of DOC and dFe were directly taken from the GEOTRACES database IDP2021, while C_T and A_T for GP16 were obtained from a published database by Bates (2018). Details of dFe and DOC distributions for GP16 were published by Resing et al. (2015), Fitzsimmons et al. (2017), and Buck et al. (2018). For cruise GA06, results for dFe were partially described by Schlosser et al. (2014), Milne et al. (2017), and Klar et al. (2018).

2.2. Seawater Carbonate Chemistry Reported on the Total Scale/IUPAC NBS Scale

pH was calculated on the total scale (pH_{tot}) using CO2SYS (Pierrot et al., 2006), a speciation model specific for seawater. We also calculated pH on the IUPAC/NBS scale (pH_{NBS}) because the ion pairing model used in

this work is dependent on stability constants taken from NIST (Smith et al., 2004), which are derived relative to the IUPAC/NBS scale. We used C_T and A_T observations from the cruises to calculate both pH_{tot} and pH_{NBS} in CO2SYS. For CO2SYS, we used constants from Mehrbach et al. (1973), refitted by Dickson and Millero (1987) and Dickson (1990), to describe the carbonate and sulfate equilibrium with H^+ ions, and from Uppström (1974) to account for boron.

2.3. Calculations of the Apparent Iron Solubility in the Ambient Water Column

The NICA-Donnan model was used to calculate dissolved Fe(III) speciation in seawater (Avendaño et al., 2016; Gledhill et al., 2015; Hiemstra & Van Riemsdijk, 2006; Zhu, Birchill, et al., 2021; Zhu, Hopwood, et al., 2021). The NICA-Donnan approach assumes that bulk properties of marine DOM can be represented by a limited number of binding site coefficients that describe intrinsic affinities between cations and different types or groups of binding sites in analogy to binding between metals and humic substances (Gledhill et al., 2022; Lodeiro et al., 2020, 2021). Briefly, the NICA model calculates the proton/metal competition within a heterogeneous mix of binding sites, with a bimodal distribution that represents more acidic groups and more basic groups (here called DOM1 and DOM2, respectively). The NICA model has three key parameters: the median value of binding affinity distributions ($\log \overline{K}$), the width of the distribution (p), and the non-ideal constants (n) that reflect both the degree of binding site heterogeneity and the binding site stoichiometry (Koopal et al., 2005). The Donnan model accounts for electrostatic interactions as a function of ionic strength and assumes that DOM is a porous gel-like substance (Koopal et al., 2020). The uniformly high ionic strength in seawater limits the impact of electrostatic effects in the ocean (Lodeiro et al., 2020; Pinheiro et al., 2021). A further key assumption is that both groups of binding sites (DOM1 and DOM2) scale proportionally with DOC. The NICA-Donnan model scales metal binding to DOC concentrations via knowledge of the moles of binding sites per kg of DOM ($Q_{(\max,\ H+,DOM1)}$ and $Q_{(\max,\ H+,DOM2)}$). We used a value of 4.07×10^{-2} kg (DOM) mol^{-1} (C) and converted DOC (μmol L^{-1}) into binding sites (kg L^{-1}) using values of 2.52 and 0.80 mol kg^{-1} for DOM1 and DOM2 respectively (Lodeiro et al., 2020).

Full details of the calculations on the speciation and solubility of Fe can be downloaded from the online protocol (Zhu et al., 2022). The NICA constants used in our calculations are provided in Supporting Information S1 (Table S1). The stability constants used in the ion-paring models are taken from NIST Standard Reference Database (Smith et al., 2004), with the exception of those for Fe. Selected equilibrium constants in critical compilations usually refer to the reference temperature $T = 298.15$ K (or 25°C) and to the standard state, that is, a pressure of 0.1 MPa (or 1 bar) and, for aqueous species, infinite dilution (ionic strength $I = 0$). Application of stoichiometric constants to solutions at the ionic strength of seawater results in systematic bias of the order of 10%–30%, dependent on the charge of the ion under consideration, since the extended Davies equation used to make the calculations is not valid above ionic strengths of 0.5 M (Gledhill et al., 2022; Turner et al., 2016). Constants for the formation of Fe hydroxide species are taken from Liu and Millero (1999). We used these constants rather than those from Liu and Millero (2002) because the former are determined in the absence of organic matter and other competing anions (e.g., sulfate) and are thus more appropriate when all the major competing interactions are independently calculated. Since we use an ion-pairing model that is based on stoichiometric constants, the equations given in Liu and Millero (1999) were transformed to the following parameters according to the Van't Hoff equation

$$K^*_{Fe(OH)3} = K_{Fe(OH)3} * 10^{(dH_{Fe(OH)3} * R_{loginv} * T_{const})} \quad (5)$$

$$R_{loginv} = 1/2.303 \times R \quad (6)$$

$$T_{const} = T_{oinv} - T_{ainv} = \frac{1}{T_0} - \frac{1}{T_{act}} \quad (7)$$

Where $K_{Fe(OH)3}$ is the equilibrium constant at temperature 283.15 K, $dH_{Fe(OH)3}$ is the enthalpy change (ΔH) of the reaction, R is the ideal gas constant, T_0 is 283.15 K, and T_{act} is the ambient seawater temperature in Kelvin (Zhu, Hopwood, et al., 2021). The variables Rloginv, Toinv, and Tainv are values that equal $\frac{1}{2.303} \times R$, $\frac{1}{T_0}$ and $\frac{1}{T_{act}}$, and are used to make the terms compatible with the software ORCHESTRA (Meeussen, 2003).

To calculate $SFe(III)_{app}$, we used a uniform concentration of total Fe(III) of 10 nmol L^{-1} in our system and allow for the formation of Fe hydroxide ($Fe(OH)_3(s)$, that is, ferrihydrite as assumed in this work). The measured dFe concentrations are not an input term for the determination of $SFe(III)_{app}$, so measured dFe concentrations and

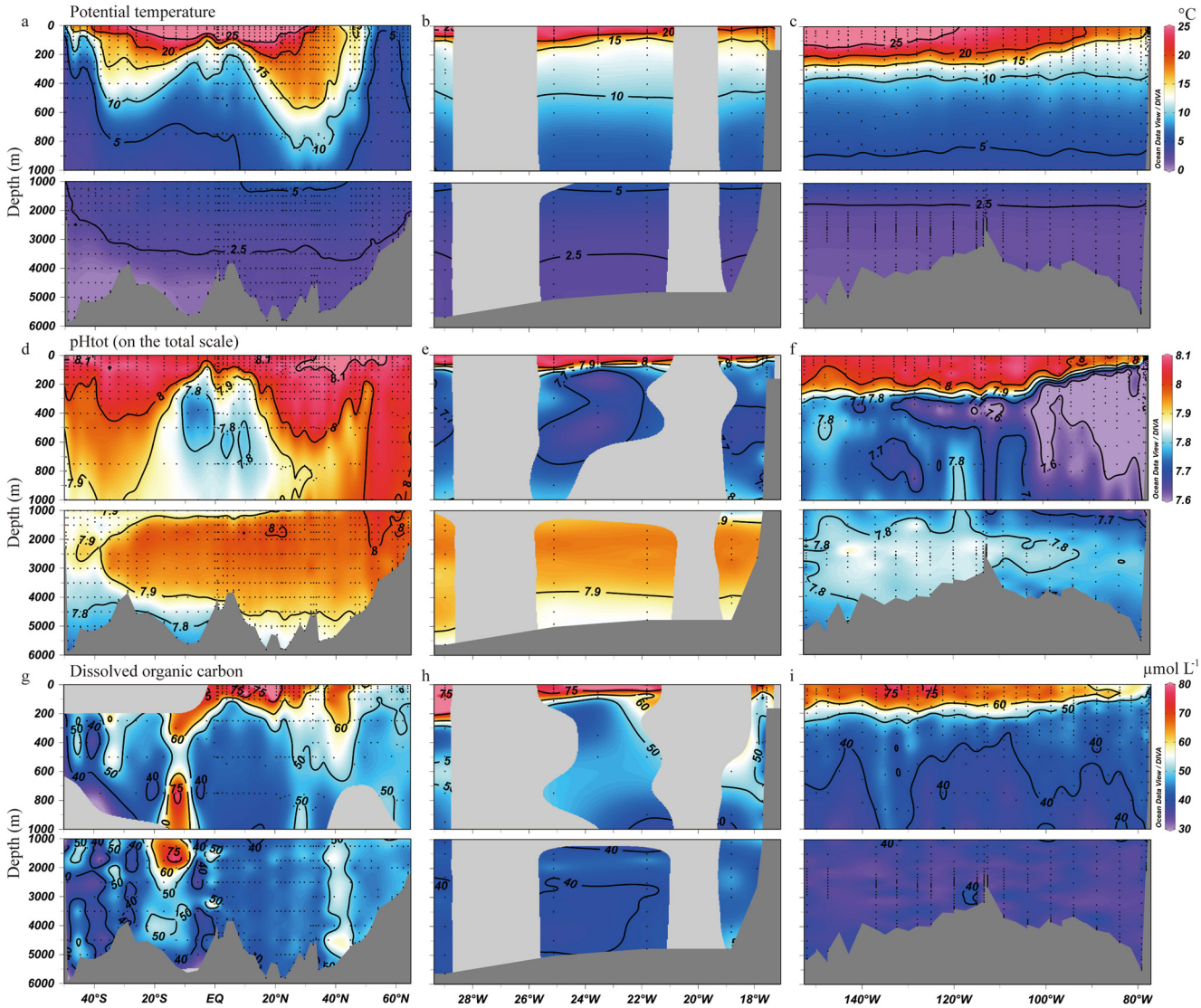

Figure 2. (a)–(c) Distributions of potential temperature collected via CTD sensor along the West Atlantic Ocean transect (GA02), Subtropical North Atlantic Ocean transect (GA06) and Southeast Pacific Ocean transect (GP16), (d)–(f) distributions of pH calculated from dissolved inorganic carbon and total alkalinity determined on the West Atlantic Ocean transect, Subtropical North Atlantic Ocean transect and Southeast Pacific Ocean transect and (g)–(i) distributions of dissolved organic carbon measured along the West Atlantic Ocean transect, Subtropical North Atlantic Ocean transect and Southeast Pacific Ocean transect.

$SFe(III)_{app}$ are independent. Initial total Fe(III) concentrations do not affect the calculated concentrations of species in the dissolved phase, as long as the initial Fe(III) concentration is set at a value high enough to ensure $Fe(OH)_3$ exceeds its solubility limit within the range of temperature and DOM concentrations observed in the study. Apparent Fe solubility is defined as the sum of dissolved inorganic and organic species (Equation 8)

$$SFe(III)_{app} = \sum Fe(OH)_i^{3-i} + Fe(III)DOM \quad (8)$$

3. Results

3.1. General Description of Seawater Physico-Chemical Conditions at the Basin Scale pH

In the top 1,000 m (Figure 2, panel d–f), ocean pH_{tot} showed higher values (>8.05) in the upper 50 m in highly productive regions of the Western North and South Atlantic as well as the Subtropical North Atlantic, compared to pH_{tot} (>8) in the Southeast Pacific. At ~100–1,000 m, ocean pH_{tot} decreased with increasing depth in the

Atlantic and Pacific Oceans, with minimum values found in the oxygen minimum zones in the Western Tropical Atlantic (<7.8), Subtropical North Atlantic (<7.7) and Southeast Pacific (<7.6). Low pH values are related to intense remineralization of sinking organic matter (Bates, 2018; Paulmier et al., 2011). Below 1,000 m, ocean pH_{tot} distribution in the West Atlantic corresponded to water masses (Rijkenberg et al., 2014), whereas pH_{tot} distributions in the Subtropical North Atlantic and Southeast Pacific were more constant, with values of 7.92 ± 0.04, $n = 43$, and 7.80 ± 0.04, $n = 232$, respectively.

3.1.1. Potential Temperature

In the top 1,000 m (Figure 2, panel a–c), potential temperature generally decreased with increasing depth in both the Atlantic and Pacific Oceans to ca. 5°C at 1,000 m. Enhanced potential temperatures (>27.5°C) were confined to the upper 100 m, between 20°S and 20°N in the West Atlantic transect and in the western part of the Southeast Pacific transect. Below 1,000 m, potential temperature slightly decreased with increasing depth in the Atlantic and Pacific Oceans, to ∼0–2.5°C at >3,500 m.

3.1.2. Dissolved Organic Carbon

In the top 1,000 m (Figure 2, panel g–i), concentrations of DOC were >80 μmol L^{-1} in the upper 50 m in the Atlantic and Pacific Oceans and decreased with increasing depth. At ∼100–1,000 m, DOC concentrations decreased from ≤80 μmol L^{-1} at ∼100 m, to values ≤50 μmol L^{-1} at ∼1,000 m in the West Atlantic and Subtropical North Atlantic, and to values ≤40 μmol L^{-1} at ∼1,000 m in the Southeast Pacific, respectively. Enhanced DOC concentrations (>60 μmol L^{-1}) were observed at ∼300–700 m between 10 and 20°S in the West Atlantic. Below 1,000 m, DOC concentrations were consistently low (∼35–50 μmol L^{-1}) in most of the West Atlantic, and slightly decreased from north (ca. 50 μmol L^{-1}) to south (ca. 40 μmol L^{-1}) following the path of the deep global thermohaline circulation. However, high DOC concentrations (>70 μmol L^{-1}) were observed at ∼1,000–2,000 m between 10 and 20°S in the West Atlantic. In the subtropical North Atlantic and Southeast Pacific, DOC concentrations were consistently low (<42 μmol L^{-1}) below 1,000 m in the water column. The distributions of DOC in both ocean basins were generally consistent with prior reported data, except for the elevated DOC concentrations in the southern part of the West Atlantic (Hansell et al., 2021).

3.2. Vertical Comparison of Apparent Iron Solubilities to Dissolved Iron Concentrations

In the West Atlantic (Figure 3, panel a), the values of calculated $SFe(III)_{app}$ were <0.6 nmol L^{-1} in the upper 200 m in the Western Tropical Atlantic and increased to ca.1.2 nmol L^{-1} at 1,000 m and toward the north (∼50–60°N). Between 1,000 and 4,000 m, which largely corresponds to the depth of North Atlantic Deep Water (Rijkenberg et al., 2014), values of $SFe(III)_{app}$ were between 1 and 1.5 nmol L^{-1}. Values of $SFe(III)_{app}$ increased to > ca. 1.6 nmol L^{-1} below 4,000 m, corresponding to the depth of Antarctic Bottom Water (Middag et al., 2018). Overall, the $SFe(III)_{app}$ was ca. 4-fold higher than observed dFe at depths less than 1,000 m, ca. 2-fold higher than the dFe between 1,000 and 4,000 m and ca. 3-fold higher than the dFe below 4,000 m (Figure 3, panel a and d). However, there were exceptions of elevated dFe concentrations as a result of lateral transport of shelf sources, remineralization in oxygen minimum zones, atmospheric dust and hydrothermal inputs (Rijkenberg et al., 2014).

In the Subtropical North Atlantic (Figure 3, panel b), calculated $SFe(III)_{app}$ showed low values (<0.6 nmol L^{-1}) in the upper 50 m in offshore waters (to the west of 20°N) and slightly increased toward the coast. At ∼100–1,000 m, the $SFe(III)_{app}$ increased with increasing depth to >1.4 nmol L^{-1} at 1,000 m. Between 1,000 and 4,000 m, the values of $SFe(III)_{app}$ were rather similar (ca. 1.2 nmol L^{-1}) in the water column. The $SFe(III)_{app}$ slightly increased to ca. 1.5 nmol L^{-1} below 4,000 m. Overall, the $SFe(III)_{app}$ was ca. 2-fold higher than observed dFe at depths less than 1,000 m and between 1,000 and 4,000 m, and ca. 3-fold higher than dFe below 4,000 m (Figure 3, panel b and e). Dissolved Fe concentrations were elevated (>1.2 nmol L^{-1}) between 100 and 1,000 m near the coast as a result of shelf-derived sedimentary inputs from the Canary current upwelling and atmospheric inputs of Fe (Rijkenberg et al., 2008). Away from coast, dFe showed a nutrient-like profile that decreased with increasing depth to <0.8 nmol L^{-1} at >1,500 m.

In the Southeast Pacific (Figure 3, panel c), values of $SFe(III)_{app}$ were <0.6 nmol L^{-1} in the upper 50 m in offshore waters (to the west of 90°W) and slightly increased toward the coast. At ∼100–1,000 m, $SFe(III)_{app}$ increased with increasing depth to ca. 1.4 nmol L^{-1} at 1,000 m. Between 1,000 and 4,000 m, $SFe(III)_{app}$ showed less variability in the water column in offshore waters but elevated concentrations up to ca. 1.8 nmol L^{-1} near the

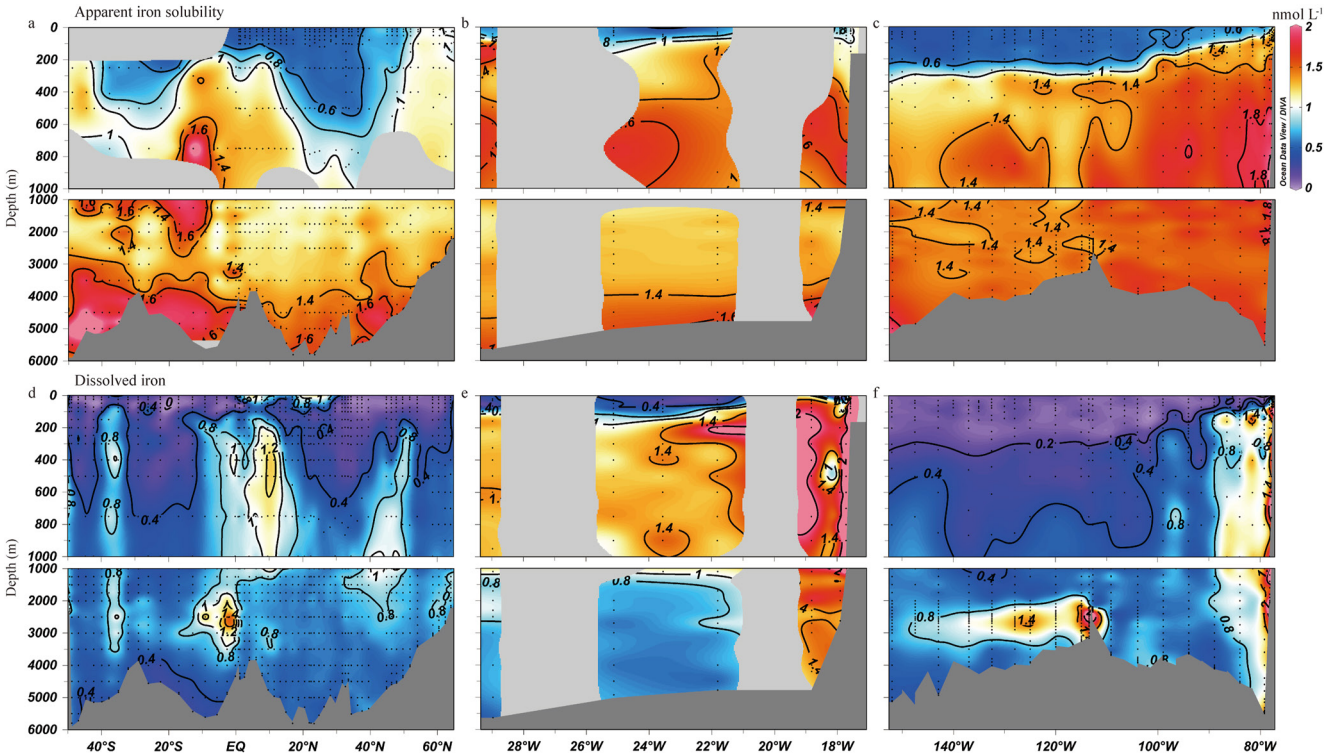

Figure 3. (a)–(c) Distributions of the apparent iron solubilities ($SFe(III)_{app}$) calculated using an ion paring-organic matter (NICA-Donnan) model at ambient seawater conditions (pH, salinity, temperature and dissolved organic carbon concentrations) during the West Atlantic Ocean transect, Subtropical North Atlantic Ocean transect and Southeast Pacific Ocean transect, and (d)–(f) distributions of dissolved iron (dFe) concentrations measured during the West Atlantic Ocean transect, Subtropical North Atlantic Ocean transect and Southeast Pacific Ocean transect.

coast. Below 4,000 m, $SFe(III)_{app}$ values slightly increased to ca. 1.5 nmol L^{-1} toward the bottom and the coast. Overall, $SFe(III)_{app}$ was ca. 4-fold higher than observed dFe at depths less than 1,000 m, ca. 2-fold higher than observed dFe between 1,000 and 4,000 m, and ca. 3-fold higher than dFe below 4,000 m (Figure 3, panel c and f). Observed dFe concentrations were elevated near the coast as a result of sedimentary inputs on the Peruvian shelf (Cutter et al., 2018; Heller et al., 2017; Rapp et al., 2020). Elevated dFe concentrations were also observed at mid depths (~2,500 m) to the west of the east Pacific Rise, and extended to the western end of the transect as a result of Fe inputs by hydrothermal vents (Fitzsimmons et al., 2017; Resing et al., 2015).

4. Discussion

In seawater, the overall Fe inventory is strongly affected by Fe(III) solubility and would be significantly lower in the absence of interactions between Fe and organic matter (Johnson et al., 1997; Liu & Millero, 2002). Furthermore, the interplay between scavenging, biological processes and solubility is poorly constrained (Tagliabue et al., 2017), and the potential impact of changes in ambient physico-chemical conditions on Fe solubility has rarely been considered (Millero et al., 2009; Ye et al., 2020; Zhu, Hopwood, et al., 2021). We calculated the apparent iron solubility ($SFe(III)_{app}$) at equilibrium, and our results predicted that $SFe(III)_{app}$ was ca. 2–4 fold higher than observed dFe concentrations. The difference between $SFe(III)_{app}$ and dFe can be ascribed to a number of factors related to both uncertainties in the parameters used in the model and the omission of processes under kinetic control that we did not account for in our equilibrium model. Uncertainties in the model arise from the parameters and the method used to calculate the activity of inorganic species in the calculations (see Methods). Furthermore, there have been relatively few determinations of NICA parameters for marine DOM (Avendaño et al., 2016; Gledhill et al., 2015; Hiemstra & Van Riemsdijk, 2006; Zhu, Birchill, et al., 2021; Zhu, Hopwood, et al., 2021) and we have assumed that NICA parameters (and by implication, DOM composition) do not change across the study areas. We also do not include an enthalpy parameter for binding of Fe to DOM, although this could have an effect on $SFe(III)_{app}$ (Liu & Millero, 2002). Our approach does not account for the effects of

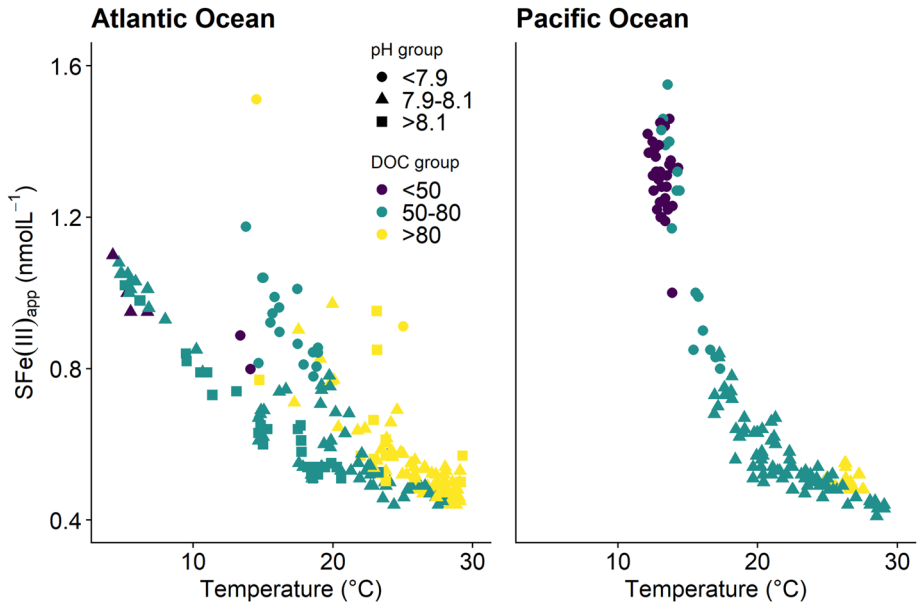

Figure 4. The apparent iron solubilities ($SFe(III)_{app}$) calculated using an ion paring-organic matter (NICA-Donnan) model at ambient seawater conditions (pH, salinity, potential temperature and dissolved organic carbon concentrations) were plotted versus temperature at depths <200 m. Points are colored according to dissolved organic carbon concentrations and shaped according to pH_{tot} (total scale).

pressure, which can also be expected to affect metal solubility (Moore & Millward, 1984). Also, non-equilibrium processes under kinetic control, such as scavenging and Fe(II) production, have not been calculated in this approach. Scavenging, via the adsorption of Fe or Fe species on the surfaces of particles, can be expected to decrease dFe concentrations since it provides a mechanism by which Fe is removed from the water column through particle sinking. On the other hand, photochemical reduction, biological reduction, or sedimentary inputs of Fe(II) will measurably enhance the dFe pool, especially in surface waters and oxygen minimum zones (Croot et al., 2019; Gonzalez-Santana et al., 2023; Laglera et al., 2022; Sarthou et al., 2011). Our results should therefore be considered within the context of these uncertainties. Nevertheless, our approach provides insight into factors influencing Fe solubility, which is linked to the changing physico-chemical state of the ocean and is an important control on Fe biogeochemistry.

4.1. Upper Limit of Apparent Iron Solubility Potentially Driven by pH and Temperature in the Upper 200 m

Using $SFe(III)_{app}$ and observed dFe in the Atlantic and Pacific Oceans, we investigated the factors that influence $SFe(III)_{app}$ at the basin scale to understand which physico-chemical parameters (pH, temperature and DOC) have the most impact on $SFe(III)_{app}$ and thus have the largest potential to further impact the dFe inventory. As shown in Figure 2, distributions of pH and temperature varied strongly in the water column at depths <200 m. The distribution of DOC showed no significant difference below 200 m (Figure 2). We thus consider a comparison of $SFe(III)_{app}$ with pH or temperature using the data collected at different depth levels in both the Atlantic and Pacific oceans.

First, a comparison of $SFe(III)_{app}$ with temperature was conducted using the data collected in the surface ocean (<200 m) with datapoints colored according to DOC concentrations, and shaped according to ambient pH_{tot} (Figure 4). Our results showed that $SFe(III)_{app}$ generally increased with decreasing temperature in the Atlantic (a West Atlantic Ocean transect and Subtropical North Atlantic Ocean transect) and Pacific (a Southeast Pacific Ocean transect in parallel to the equator) Oceans since the formation of $Fe(OH)_3(s)$ is exothermic and is inhibited by increased temperatures (Liu & Millero, 1999). The $SFe(III)_{app}$ value was ca. 0.4 nmol L^{-1} at the highest temperatures (~27–29°C) observed in the study areas. The $SFe(III)_{app}$ was higher (>1.2 nmol L^{-1}) at lower temperature (ca. 13°C) with additional impacts from pH in the Pacific Ocean. $SFe(III)_{app}$ was higher (>1.2 nmol L^{-1}) at both lower (<8°C) and medium temperature (~13–17°C) with additional impacts by both pH and DOC in the

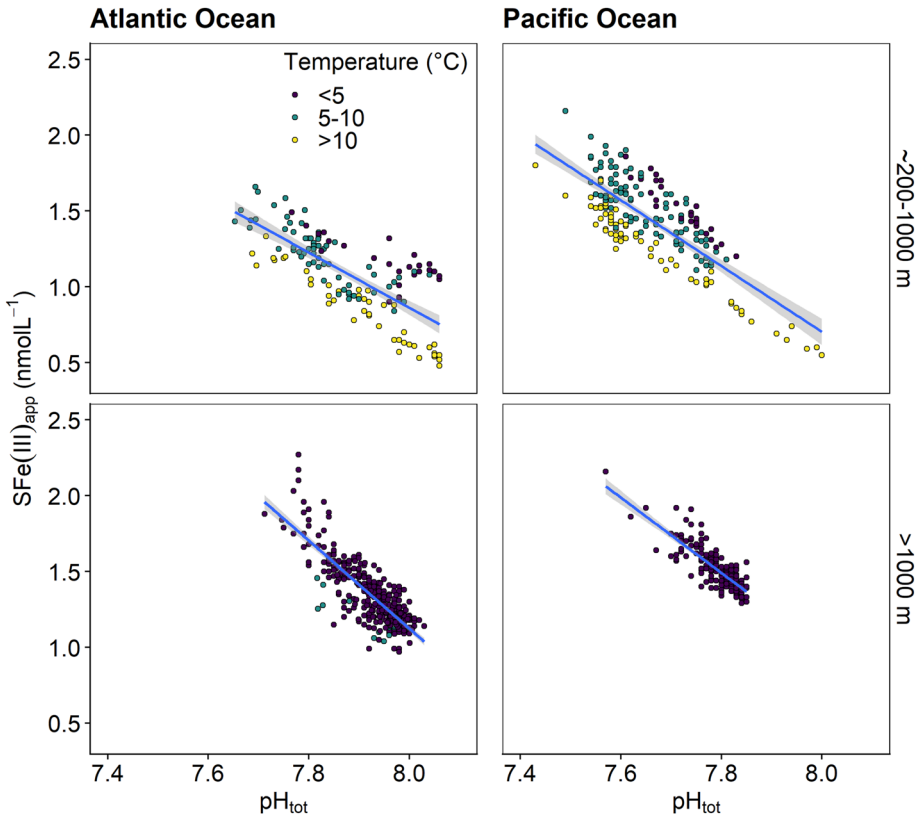

Figure 5. The apparent iron solubilities ($SFe(III)_{app}$) calculated using an ion paring-organic matter (NICA-Donnan) model at ambient seawater conditions (pH, salinity, potential temperature and dissolved organic carbon concentrations) plotted versus pH_{tot} (total scale) at depths >200 m. Points are colored according to temperature.

Atlantic Ocean. This is understandable, since lower pH_{tot} (<7.9) as a result of strong remineralization in the Subtropical North Atlantic enhances Fe(III) solubility (Millero et al., 2009; Zhu, Hopwood, et al., 2021) and the highly productive regions of the Subtropical North Atlantic also yield high DOC and thereby increase the number of DOM binding sites (Zhu, Birchill, et al., 2021) in the moderate temperature range (~13–17°C). Lower temperatures enhanced the solubility of Fe hydroxide ($Fe(OH)_3(s)$), resulted in more free Fe^{3+} bound to OH^- and DOM1- or DOM2-type groups in marine DOM and thus increased $SFe(III)_{app}$ (Liu & Millero, 2002). In waters <200 m deep, all three parameters (temperature, pH and DOC) therefore act in concert to influence $SFe(III)_{app}$. Furthermore, the individual contributions of pH and temperature cannot be fully disentangled since low temperatures enhance the solubility of CO_2 and therefore impact seawater pH.

4.2. Both pH and Temperature Affect the Apparent Iron Solubility Below the Surface Ocean

A comparison of $SFe(III)_{app}$ with pH was conducted using the data collected at >200 m (Figure 5). As shown in Figure 2, DOC concentrations were rather constant (41.9 ± 6.2 μmol L^{-1}, n = 1,085) at depths >200 m. Our results showed that $SFe(III)_{app}$ increased with decreasing pH_{tot} for the Atlantic and Pacific cruises, including intermediate (~200–1,000 m) to deep waters (>1,000 m). The negative slopes for pH-$SFe(III)_{app}$ were different for the Atlantic and Pacific Oceans, and decreased from intermediate (Atlantic Ocean: $y = -1.82 \pm 0.14X + 15.4 \pm 1.11$, $r^2 = 0.56$; Pacific Ocean: $y = -2.26 \pm 0.13X + 18.8 \pm 0.98$, $r^2 = 0.63$) to deep waters (Atlantic Ocean: $y = -2.9 \pm 0.11X + 24.3 \pm 0.83$, $r^2 = 0.67$; Pacific Ocean: $y = -2.42 \pm 0.12X + 20.4 \pm 0.96$, $r^2 = 0.66$). These differences between slopes for pH-$SFe(III)_{app}$ likely reflect the relative changes in temperature distributions (Byrne et al., 2000; Liu & Millero, 2002). Our results suggest that the increase in $SFe(III)_{app}$ with decreasing pH as a result of, for example, ocean acidification or increased remineralization in eastern boundary upwelling regions would be mitigated by lower solubility of Fe hydroxide in warmer seawaters. This impact of pH on the $SFe(III)_{app}$ is consistent with observations of increased dFe concentrations with decreasing pH in the presence of excess particulate Fe in a coastal mesocosm experiment (Breitbarth et al., 2010).

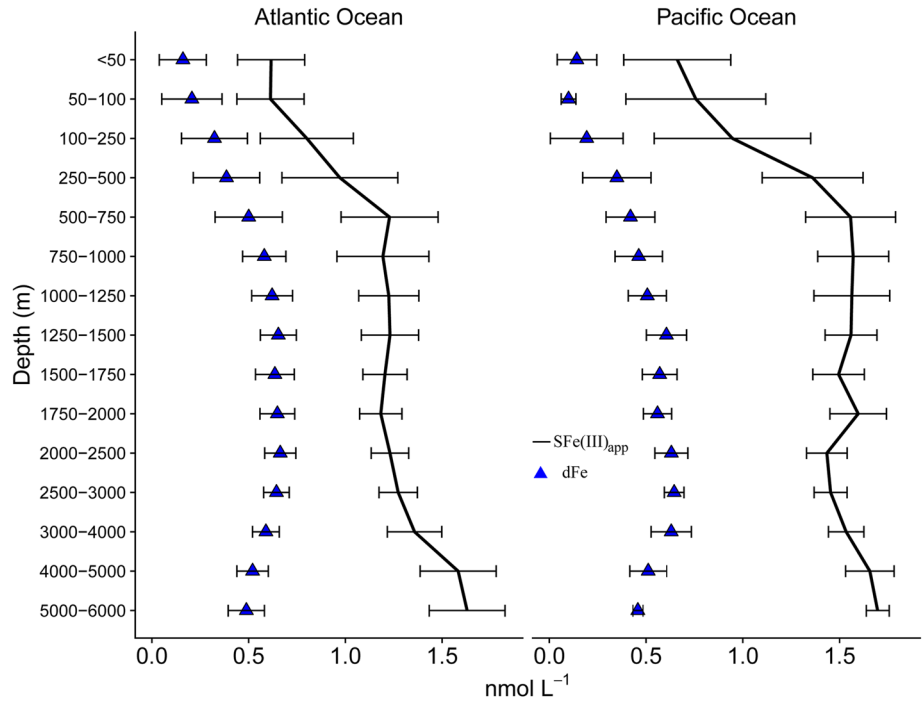

Figure 6. The vertical distributions of horizontally averaged calculated apparent iron solubility ($SFe(III)_{app}$, black solid lines) at ambient seawater conditions and measured dissolved iron concentration (dFe, blue triangle points) in the Atlantic (a West Atlantic transect: at latitude ~49°S–64°N; a Subtropical Atlantic transect: at latitude ~12°N and longitude ~17–29°W) and Pacific (a Southeastern Pacific transect: at longitude ~77–152°W) oceans. We omitted dFe profiles that were strongly influenced by source signatures from for example, hydrothermal vents, atmospheric dust and suboxic sediment inputs in both ocean basins (Fitzsimmons et al., 2017; Resing et al., 2015; Rijkenberg et al., 2014) (Table S2 in Supporting Information S1).

4.3. Vertical Distributions of Dissolved Iron Concentrations Determined by Changes in Apparent Iron Solubility

Overall, the values of $SFe(III)_{app}$ were ca. 3-fold higher than dFe concentrations in the water columns of the Atlantic and Pacific Oceans (Figure 3). The similarities and differences between dFe and $SFe(III)_{app}$ in both ocean basins largely reflected the strong influence of point sources on the dFe distribution (e.g., shelf, atmospheric and hydrothermal inputs) (Rapp et al., 2020; Resing et al., 2015; Rijkenberg et al., 2014) or removal process (e.g., scavenging or biological uptake) (Boyd et al., 2005; Tagliabue et al., 2019). However, the distributions of dFe showed a correspondence to the changes in $SFe(III)_{app}$, particularly when considering the vertical distributions. This confirms earlier findings that dFe depth profiles are influenced by Fe(III) hydroxide solubility, in addition to remineralization and scavenging (Johnson et al., 1997; Kuma et al., 2003; Liu & Millero, 2002; Tagliabue et al., 2014). To further explore this comparison, we considered horizontally averaged dFe and $SFe(III)_{app}$ depth profiles in the Atlantic Ocean (n = 1,079 and 798 data points for dFe and $SFe(III)_{app}$, respectively) and the Pacific Ocean (n = 492 and 555 data points for dFe and $SFe(III)_{app}$, respectively) (Figure 6). We omitted dFe profiles that were strongly influenced by source signatures from for example, hydrothermal vents, atmospheric dust and sediment inputs in both ocean basins, according to earlier descriptions by Rijkenberg et al. (2014), Milne et al. (2017), and Fitzsimmons et al. (2017) (Table S2 in Supporting Information S1).

We observed similar trends in the vertical distributions of horizontally averaged dFe and $SFe(III)_{app}$ in the top 1,000 m in the Pacific and Atlantic Oceans, with both dFe and $SFe(III)_{app}$ showing regeneration-like depth profiles. The vertical distributions of averaged dFe and $SFe(III)_{app}$ were rather constant at depths between 1,000 and 4,000 m. At >4,000 m, the averaged $SFe(III)_{app}$ increased with increasing depth up to 1.6 nmol L^{-1}, while averaged dFe decreased at depths >4,000 m. Differences between dFe and $SFe(III)_{app}$ in surface waters (<200 m) are likely associated with biological activity, whilst the waters at depths >4,000 m are strongly influenced by Antarctic Bottom Waters, which are cold and hence have higher $SFe(III)_{app}$ but are depleted in dFe because they are formed in the Southern Ocean (Rijkenberg et al., 2014), which is known to have lower iron supplies relative to

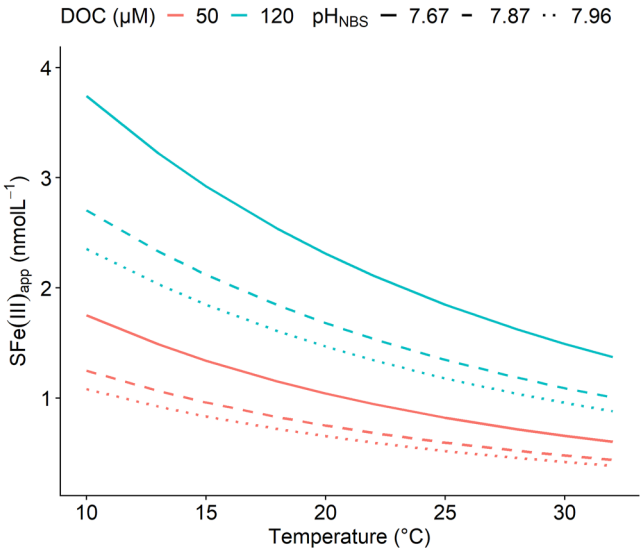

Figure 7. Sensitivity of SFe(III)$_{app}$ to changing pH, temperature and dissolved organic carbon conditions with constant salinity (35). We initiate calculations with 10 nmol L^{-1} total Fe(III) in the model system with different temperatures, dissolved organic carbon and pH$_{tot}$ (total scale) under lower, medium and higher emission scenarios by the end of this century (Jiang et al., 2019) to represent dynamics of the surface dissolved iron (dFe) inventory in the context of a warming and acidifying ocean and calculate the apparent iron solubility (SFe(III)$_{app}$) using an ion paring-organic matter (NICA-Donnan) model.

other ocean basins (Tagliabue et al., 2017). However, additional factors may also influence differences in trends observed for dFe and SFe(III)$_{app}$. Consistent with prior work, we used ferrihydrite formation to represent a component of scavenging, that is, dFe is removed from the ambient water column when exceeding the solubility of iron at equilibrium. Unlike the kinetically implemented scavenging process in global biogeochemical models with assumed ligand concentrations and binding capacities (Voelker & Tagliabue, 2015), SFe(III)$_{app}$ and the formation of ferrihydrite reflect the changing seawater chemistry on the upper limit of Fe availability determined by both Fe solubility and organic complexation. However, the solubility constants of Fe hydroxide, applied in our calculations here, are representative of relatively fresh (1 week old) precipitates and thus comprise an upper limit for Fe solubility in seawater (Byrne et al., 2000; Liu & Millero, 2002). Aging of ferrihydrite leads to conformational changes within the minerals or "hardening" that decreases solubility with time (Raiswell et al., 2010).

Furthermore, a key assumption in these calculations is that the binding sites of DOM used in the ion paring-organic matter (NICA-Donnan) model scale proportionally with DOC. For example, in surface waters, changes in acid-base and Fe-binding properties of the DOM pool as a result of enhanced primary production could invalidate the assumption that binding sites scale to DOC (Lodeiro et al., 2021; Zhu, Birchill, et al., 2021). In addition, although a major fraction of the marine DOM pool is thought to be recalcitrant, especially in older deep waters (Hansell, 2013), the diversity of functional groups is likely to be subject to spatial and temporal changes (Hansman et al., 2015; Medeiros et al., 2015). Such variability could result in differences in SFe(III)$_{app}$ since the NICA constants used to calculate SFe(III)$_{app}$ in this work were derived from titrations undertaken on samples from waters collected at depths <800 m (Lodeiro et al., 2021; Zhu, Hopwood, et al., 2021).

4.4. Environmental Implications in a Warmer and More Acidifying Ocean

Information on the speciation and solubility of Fe at ambient seawater conditions is crucial to fully understand the biogeochemical processes which moderate Fe availability to biota and thus affect the marine carbon cycle (Boyd & Ellwood, 2010; Tagliabue et al., 2017). A few studies have addressed the impact of decreasing pH as a result of ocean acidification on trace metal speciation. Millero et al. (2009), using a Pitzer interaction model, examined the effect of ocean acidification on inorganic complexation of trace metals and found a 40% increase in the solubility of inorganic Fe(III) when pH$_{NBS}$ decreased from 8.1 to 7.4. Gledhill et al. (2015) and Stockdale et al. (2016) used the ion-paring organic matter (NICA-Donnan or WHAM/Model VII) models to investigate changes in the organic complexation of Fe that dominate the control of Fe speciation and inorganic complexation and indicated that Fe may become more available for marine organisms as a consequence of ocean acidification. Our results also suggest that projected decreases in pH as a result of ocean acidification would lead to further overall increases in SFe(III)$_{app}$. Here, we conducted a sensitivity test to further provide insights into how changes in pH, temperature and DOC may interact to affect SFe(III)$_{app}$ in a future ocean. According to Jiang et al. (2019), using IPCC data for pCO_2 and pH under lower (RCP2.6), medium (RCP4.5) and higher (RCP8.5) emission scenarios by the end of this century (pH$_{tot}$ decreasing by an average of about ~0.04, 0.13, or 0.33, respectively), we plotted the calculated SFe(III)$_{app}$ against temperature at both lower (~50 μmol L^{-1}) and higher (~120 μmol L^{-1}) DOC concentrations for the surface ocean (Figure 7).

Our results showed that the SFe(III)$_{app}$ ranged from 0.39 nmol L^{-1} at pH$_{NBS}$ 7.96, T = 32°C, DOC = 50 μmol L^{-1}–3.74 nmol L^{-1} at pH$_{NBS}$ 7.67, T = 10°C, DOC = 120 μmol L^{-1}. At lower DOC = 50 μmol L^{-1} and temperatures between 20 and 30°C (e.g., surface water in subtropical gyres), the SFe(III)$_{app}$ decreased by an average 11% with a 2°C temperature increase (i.e., expected in a warmer ocean) at each pH value. At higher DOC = 150 μmol L^{-1} and temperatures between 20 and 30°C, the SFe(III)$_{app}$ decreased by an average 10% with a 2°C temperature increase at each pH value. However for both DOC scenarios/concentrations, a pH decrease of ~0.33 unit would increase

the $SFe(III)_{app}$ by an average 37% at each temperature value. The impact of pH on Fe speciation and solubility is nearly 3-times higher than that of temperature, whereas different DOC concentration scenarios have minimal impact over the range of values considered. We further analysed the distribution of both inorganic and organic fractions of calculated $SFe(III)_{app}$ with response to changing pH, temperature and DOC scenarios. Our results showed Fe(III) bound to organic matter made up 81%–96% of $SFe(III)_{app}$ and increased with increasing DOC concentrations but decreasing temperature and pH and indicate that $SFe(III)_{app}$ would be significantly elevated in, for example, an acidifying and warmer ocean. Nevertheless, since the enthalpy of formation for Fe binding to DOM is not accounted for in our calculations, the overall trend in Fe solubility in a warmer, acidifying ocean is still subject to uncertainty (Liu & Millero, 2002).

5. Conclusions

We derived apparent iron solubility at ambient seawater pH, temperature and DOC concentrations, using an ion paring-organic matter (NICA-Donnan) model by applying newly derived proton/Fe(III) NICA constants for marine DOM. We compared calculated $SFe(III)_{app}$ to measured dFe concentrations that were obtained during three GEOTRACES cruises in the Atlantic and Pacific Oceans. Our results show that the distributions of dFe showed some correspondence to relative changes in $SFe(III)_{app}$, particularly when considering the vertical distributions at depths above 4,000 m. We further investigated the physico-chemical parameters (pH, temperature and DOC) influencing the $SFe(III)_{app}$ on a basin scale. Our results showed that temperature impacts the upper limit of $SFe(III)_{app}$ in the surface ocean with further impacts of pH and DOC concentrations, while both pH and temperature impact $SFe(III)_{app}$ in the deep ocean. Our comparison of the vertical distributions of horizontally averaged dFe and $SFe(III)_{app}$ indicates that vertical dFe distributions are underpinned by changes in $SFe(III)_{app}$, which are driven by relative changes in ambient pH and temperature, in addition to processes such as scavenging and remineralization. The results of the sensitivity test reaffirm that consideration of the impact of changes in ambient pH and temperature is important for Fe cycling, especially in the context of an acidifying and warming ocean. Nevertheless, our results should be interpreted within the context of uncertainties arising from the modeling approach in terms of parameter availability and calculations of activity, and from scavenging and redox processes that are under kinetic control. In particular, further work to constrain acid-base properties and enthalpies of marine DOM, and the solubility constants for Fe hydroxide is required to increase confidence in the predictions resulting from such approaches.

Data Availability Statement

All data reported in this study are available at PANGAEA open access repository (https://doi.pangaea.de/10.1594/PANGAEA.952541). Data of depth, potential temperature (in the ITS-90 convention) and practical salinity for GA02, GA06, and GP16 have been included in the GEOTRACES database IDP2021 (GEOTRACES Intermediate Data Product Group, 2021). Data of dissolved inorganic carbon (C_T), total alkalinity (A_T), dissolved organic carbon (DOC) and dissolved Fe (dFe) for GA02 have been included in the GEOTRACES database IDP2021. Data of DOC and dFe for GP16 have been included in the GEOTRACES database IDP2021.

Map of the study area (Figure 1) and section plots (Figures 2 and 3) were made using Ocean Data View software and DIVA gridding calculations (Schlitzer, 2023). Figures 4–7 were made using open source R statistical programming (Version 4.2.0) (https://www.r-project.org/) and RStudio (https://posit.co/) with the code *ggplot2* (https://github.com/hadley/ggplot2-book). Software- pH is calculated from C_T and A_T on both the total scale and the NBS scale using CO2SYS (Pierrot et al., 2006). Software- the apparent iron solubility is calculated using an ion paring-organic matter (NICA-Donnan) model using the speciation code ORCHESTRA (Meeussen, 2003). All codes are described in an online protocol (Zhu et al., 2022).

Acknowledgments
We thank the captain and crew of RRS Discovery throughout cruise GA06 (D361). We also thank Santiago Gonzalez for measuring dissolved organic carbon during the cruise GA02. We acknowledge Prof. D. A. Hansell for making the compilation of dissolved organic carbon in seawater available, and the GEOTRACES community for making their dissolved iron data available. The research project for the RRS Discovery D361 cruise was funded by the UK National Environmental Research Council (NE/G015732/1). This work is funded by The Helmholtz Association and DFG project GL 807/2-1 awarded to M. Gledhill. K.Z. is grateful to the China Scholarship Council for providing financial support. Open Access funding enabled and organized by Projekt DEAL.

References

Avendaño, L., Gledhill, M., Achterberg, E. P., Rérolle, V. M. C., & Schlosser, C. (2016). Influence of ocean acidification on the organic complexation of iron and copper in Northwest European shelf seas; a combined observational and model study. *Frontiers in Marine Science*, *3*. https://doi.org/10.3389/fmars.2016.00058

Bates, N. R. (2018). Seawater carbonate chemistry distributions across the Eastern South Pacific Ocean sampled as part of the GEOTRACES project and changes in marine carbonate chemistry over the past 20 years. *Frontiers in Marine Science*, *5*. https://doi.org/10.3389/fmars.2018.00398

Boyd, P. W., & Ellwood, M. J. (2010). The biogeochemical cycle of iron in the ocean. *Nature Geoscience*, *3*(10), 675–682. https://doi.org/10.1038/ngeo964

Boyd, P. W., Jickells, T., Law, C. S., Blain, S., Boyle, E. A., Buesseler, K. O., et al. (2007). Mesoscale iron enrichment experiments 1993-2005: Synthesis and future directions. *Science*, *315*(5812), 612–617. https://doi.org/10.1126/science.1131669

Boyd, P. W., Law, C. S., Hutchins, D. A., Abraham, E. R., Croot, P. L., Ellwood, M., et al. (2005). FeCycle: Attempting an iron biogeochemical budget from a mesoscale SF6tracer experiment in unperturbed low iron waters. *Global Biogeochemical Cycles*, *19*(4). https://doi.org/10.1029/2005gb002494

Breitbarth, E., Bellerby, R. J., Neill, C. C., Ardelan, M. V., Meyerhöfer, M., Zöllner, E., et al. (2010). Ocean acidification affects iron speciation during a coastal seawater mesocosm experiment. *Biogeosciences*, *7*(3), 1065–1073. https://doi.org/10.5194/bg-7-1065-2010

Buck, K. N., Sedwick, P. N., Sohst, B., & Carlson, C. A. (2018). Organic complexation of iron in the eastern tropical South Pacific: Results from US GEOTRACES Eastern Pacific Zonal Transect (GEOTRACES cruise GP16). *Marine Chemistry*, *201*, 229–241. https://doi.org/10.1016/j.marchem.2017.11.007

Buck, K. N., Sohst, B., & Sedwick, P. N. (2015). The organic complexation of dissolved iron along the US GEOTRACES (GA03) North Atlantic Section. *Deep Sea Research Part II: Topical Studies in Oceanography*, *116*, 152–165. https://doi.org/10.1016/j.dsr2.2014.11.016

Byrne, R. H., Luo, Y.-R., & Young, R. W. (2000). Iron hydrolysis and solubility revisited: Observations and comments on iron hydrolysis characterizations. *Marine Chemistry*, *70*(1–3), 23–35. https://doi.org/10.1016/S0304-4203(00)00012-8

Croot, P. L., Heller, M. I., & Wuttig, K. (2019). Redox processes impacting the flux of iron(II) from shelf sediments to the OMZ along the Peruvian shelf. *ACS Earth and Space Chemistry*, *3*(4), 537–549. https://doi.org/10.1021/acsearthspacechem.8b00203

Cutter, G., Moffett, J. G., Nielsdottir, M. C., & Sanial, V. (2018). Multiple oxidation state trace elements in suboxic waters off Peru: In situ redox processes and advective/diffusive horizontal transport. *Marine Chemistry*, *201*, 77–89. https://doi.org/10.1016/j.marchem.2018.01.003

Dickson, A. G. (1990). Standard potential of the reaction: $AgCl(s) + 12H_2(g) = Ag(s) + HCl(aq)$, and and the standard acidity constant of the ion $HSO4^-$ in synthetic sea water from 273.15 to 318.15 K. *The Journal of Chemical Thermodynamics*, *22*(2), 113–127. https://doi.org/10.1016/0021-9614(90)90074-Z

Dickson, A. G., & Millero, F. J. (1987). A comparison of the equilibrium constants for the dissociation of carbonic acid in seawater media. *Deep Sea Research Part A. Oceanographic Research Papers*, *34*(10), 1733–1743. https://doi.org/10.1016/0198-0149(87)90021-5

Fitzsimmons, J. N., John, S. G., Marsay, C. M., Hoffman, C. L., Nicholas, S. L., Toner, B. M., et al. (2017). Iron persistence in a distal hydrothermal plume supported by dissolved-particulate exchange. *Nature Geoscience*, *10*(3), 195–201. https://doi.org/10.1038/Ngeo2900

Garcia-Soto, C., Cheng, L., Caesar, L., Schmidtko, S., Jewett, E. B., Cheripka, A., et al. (2021). An overview of ocean climate change indicators: Sea surface temperature, ocean heat content, ocean pH, dissolved oxygen concentration, Arctic Sea Ice extent, thickness and volume, Sea level and strength of the AMOC (Atlantic Meridional Overturning Circulation). *Frontiers in Marine Science*, *8*. https://doi.org/10.3389/fmars.2021.642372

GEOTRACES Intermediate Data Product Group. (2021). The GEOTRACES intermediate data product 2021 (IDP2021) [Dataset]. NERC EDS British Oceanographic Data Centre NOC. https://doi.org/10.5285/cf2d9ba9-d51d-3b7c-e053-8486abc0f5fd

Gerringa, L. J. A., Rijkenberg, M. J. A., Schoemann, V., Laan, P., & De Baar, H. J. W. (2015). Organic complexation of iron in the West Atlantic Ocean. *Marine Chemistry*, *177*, 434–446. https://doi.org/10.1016/j.marchem.2015.04.007

Gledhill, M., Achterberg, E. P., Li, K., Mohamed, K. N., & Rijkenberg, M. J. A. (2015). Influence of ocean acidification on the complexation of iron and copper by organic ligands in estuarine waters. *Marine Chemistry*, *177*, 421–433. https://doi.org/10.1016/j.marchem.2015.03.016

Gledhill, M., & Buck, K. N. (2012). The organic complexation of iron in the marine environment: A review. *Frontiers in Microbiology*, *3*. https://doi.org/10.3389/fmicb.2012.00069

Gledhill, M., Hollister, A., Seidel, M., Zhu, K., Achterberg, E. P., Dittmar, T., & Koschinsky, A. (2022). Trace metal stoichiometry of dissolved organic matter in the Amazon plume. *Science Advances*, *8*(31). https://doi.org/10.1126/sciadv.abm2249

Gonzalez-Santana, D., Lough, A. J. M., Planquette, H., Sarthou, G., Tagliabue, A., & Lohan, M. C. (2023). The unaccounted dissolved iron (II) sink: Insights from dFe(II) concentrations in the deep Atlantic Ocean. *Science of the Total Environment*, *862*, 161179. https://doi.org/10.1016/j.scitotenv.2022.161179

Hansell, D. A. (2013). Recalcitrant dissolved organic carbon fractions. *Annual Review of Marine Science*, *5*(1), 421–445. https://doi.org/10.1146/annurev-marine-120710-100757

Hansell, D. A., Carlson, C. A., Amon, R. M. W., Álvarez-Salgado, X. A., Yamashita, Y., Romera-Castillo, C., & Bif, M. B. (2021). Compilation of dissolved organic matter (DOM) data obtained from the global ocean surveys from 1994 to 2020 (NCEI Accession 0227166) [Indicate subset used] [Dataset]. https://doi.org/10.25921/s4f4-ye35

Hansman, R. L., Dittmar, T., & Herndl, G. J. (2015). Conservation of dissolved organic matter molecular composition during mixing of the deep water masses of the northeast Atlantic Ocean. *Marine Chemistry*, *177*, 288–297. https://doi.org/10.1016/j.marchem.2015.06.001

Heller, M. I., Lam, P. J., Moffett, J. W., Till, C. P., Lee, J.-M., Toner, B. M., & Marcus, M. A. (2017). Accumulation of Fe oxyhydroxides in the Peruvian oxygen deficient zone implies non-oxygen dependent Fe oxidation. *Geochimica et Cosmochimica Acta*, *211*, 174–193. https://doi.org/10.1016/j.gca.2017.05.019

Hiemstra, T., & Van Riemsdijk, W. H. (2006). Biogeochemical speciation of Fe in ocean water. *Marine Chemistry*, *102*(3–4), 181–197. https://doi.org/10.1016/j.marchem.2006.03.008

IPCC. (2013). In T. F. Stocker, D. Qin, G.-K. Plattner, M. Tignor, S. K. Allen, et al. (Eds.), *Climate change 2013: The physical science basis. Contribution of working group I to the fifth assessment report of the intergovernmental panel on climate change* (p. 1535). Cambridge University Press.

Jiang, L.-Q., Carter, B. R., Feely, R. A., Lauvset, S. K., & Olsen, A. (2019). Surface ocean pH and buffer capacity: Past, present and future. *Scientific Reports*, *9*(1), 18624. https://doi.org/10.1038/s41598-019-55039-4

Johnson, K. S., Gordon, R. M., & Coale, K. H. (1997). What controls dissolved iron concentrations in the world ocean? *Marine Chemistry*, *57*(3–4), 137–161. https://doi.org/10.1016/S0304-4203(97)00043-1

Kinniburgh, D. G., Van Riemsdijk, W. H., Koopal, L. K., Borkovec, M., Benedetti, M. F., & Avena, M. J. (1999). Ion binding to natural organic matter: Competition, heterogeneity, stoichiometry and thermodynamic consistency. *Colloids and Surfaces A: Physicochemical and Engineering Aspects*, *151*(1–2), 147–166. https://doi.org/10.1016/S0927-7757(98)00637-2

Klar, J. K., Schlosser, C., Milton, J. A., Woodward, E. M. S., Lacan, F., Parkinson, I. J., et al. (2018). Sources of dissolved iron to oxygen minimum zone waters on the Senegalese continental margin in the tropical North Atlantic Ocean: Insights from iron isotopes. *Geochimica et Cosmochimica Acta*, *236*, 60–78. https://doi.org/10.1016/j.gca.2018.02.031

Koopal, L. K., Saito, T., Pinheiro, J. P., & Van Riemsdijk, W. H. (2005). Ion binding to natural organic matter: General considerations and the NICA–Donnan model. *Colloids and Surfaces a Physicochemical and Engineering Aspects*, *265*(1–3), 40–54. https://doi.org/10.1016/j.colsurfa.2004.11.050

Koopal, L. K., Tan, W., & Avena, M. (2020). Equilibrium mono- and multicomponent adsorption models: From homogeneous ideal to heterogeneous non-ideal binding. *Advances in Colloid and Interface Science*, *280*, 102138. https://doi.org/10.1016/j.cis.2020.102138

Kuma, K., Isoda, Y., & Nakabayashi, S. (2003). Control on dissolved iron concentrations in deep waters in the western North Pacific: Iron(III) hydroxide solubility. *Journal of Geophysical Research*, *108*(C9), 3289. https://doi.org/10.1029/2002jc001481

Laglera, L. M., Uskaikar, H., Klaas, C., Naqvi, S. W. A., Wolf-Gladrow, D. A., & Tovar-Sanchez, A. (2022). Dissolved and particulate iron redox speciation during the LOHAFEX fertilization experiment. *Marine Pollution Bulletin*, *184*, 114161. https://doi.org/10.1016/j.marpolbul.2022.114161

Liu, X., & Millero, F. J. (1999). The solubility of iron hydroxide in sodium chloride solutions. *Geochimica et Cosmochimica Acta*, *63*(19–20), 3487–3497. https://doi.org/10.1016/S0016-7037(99)00270-7

Liu, X., & Millero, F. J. (2002). The solubility of iron in seawater. *Marine Chemistry*, *77*(1), 43–54. https://doi.org/10.1016/S0304-4203(01)00074-3

Lodeiro, P., Rey-Castro, C., David, C., Achterberg, E. P., Puy, J., & Gledhill, M. (2020). Acid-base properties of dissolved organic matter extracted from the marine environment. *Science of the Total Environment*, *729*, 138437. https://doi.org/10.1016/j.scitotenv.2020.138437

Lodeiro, P., Rey-Castro, C., David, C., Puy, J., Achterberg, E. P., & Gledhill, M. (2021). Seasonal variations in proton binding characteristics of dissolved organic matter isolated from the southwest Baltic Sea. *Environmental Science & Technology*, *55*(23), 16215–16223. https://doi.org/10.1021/acs.est.1c04773

Medeiros, P. M., Seidel, M., Powers, L. C., Dittmar, T., Hansell, D. A., & Miller, W. L. (2015). Dissolved organic matter composition and photochemical transformations in the northern North Pacific Ocean. *Geophysical Research Letters*, *42*(3), 863–870. https://doi.org/10.1002/2014GL062663

Meeussen, J. C. L. (2003). ORCHESTRA: An object-oriented framework for implementing chemical equilibrium models [Software]. Environmental Science & Technology, *37*, 1175–1182. https://doi.org/10.1021/es025597s

Mehrbach, C., Culberson, C. H., Hawley, J. E., & Pytkowicx, R. M. (1973). Measurement of the apparent dissociation constants of carbonic acid in seawater at atmospheric pressure. *Limnology & Oceanography*, *18*(6), 897–907. https://doi.org/10.4319/lo.1973.18.6.0897

Middag, R., Van Heuven, S. M. A. C., Bruland, K. W., & De Baar, H. J. W. (2018). The relationship between cadmium and phosphate in the Atlantic Ocean unravelled. *Earth and Planetary Science Letters*, *492*, 79–88. https://doi.org/10.1016/j.epsl.2018.03.046

Millero, F. J., Woosley, R., Ditrolio, B., & Waters, J. (2009). Effect of ocean acidification on the speciation of metals in seawater. *Oceanography*, *22*(4), 72–85. https://doi.org/10.5670/oceanog.2009.98

Milne, A., Schlosser, C., Wake, B. D., Achterberg, E. P., Chance, R., Baker, A. R., et al. (2017). Particulate phases are key in controlling dissolved iron concentrations in the (sub)tropical North Atlantic. *Geophysical Research Letters*, *44*(5), 2377–2387. https://doi.org/10.1002/2016GL072314

Moore, R. M., & Millward, G. E. (1984). Dissolved-particulate interactions of aluminum in ocean waters. *Geochimica et Cosmochimica Acta*, *48*(2), 235–241. https://doi.org/10.1016/0016-7037(84)90247-3

Paulmier, A., Ruiz-Pino, D., & Garçon, V. (2011). CO_2 maximum in the oxygen minimum zone (OMZ). *Biogeosciences*, *8*(2), 239–252. https://doi.org/10.5194/bg-8-239-2011

Perdue, E. M. (1985). Acidic functional groups in humic substances. In G. R. Aiken, D. M. McKnight, R. L. Wershaw, & P. MacCarthy (Eds.), *Humic substances in soil, sediment, and water: Geochemistry, isolation, and characterization* (pp. 493–526), Wiley-Interscience.

Perdue, E. M., & Lytle, C. R. (1983). A distribution model for binding of protons and metal ions by humic substances. *Environmental Science & Technology*, *17*(11), 654–660. https://doi.org/10.1021/es00117a006

Pierrot, D. E., Lewis, E., & Wallace, D. W. R. (2006). MS excel program developed for CO_2 system calculations. ORNL/CDIAC-105a [Software]. https://doi.org/10.3334/CDIAC/otg.CO2SYS_XLS_CDIAC105a

Pinheiro, J. P., Rotureau, E., & Duval, J. F. L. (2021). Addressing the electrostatic component of protons binding to aquatic nanoparticles beyond the Non-Ideal Competitive Adsorption (NICA)-Donnan level: Theory and application to analysis of proton titration data for humic matter. *Journal of Colloid and Interface Science*, *583*, 642–651. https://doi.org/10.1016/j.jcis.2020.09.059

Raiswell, R., Vu, H. P., Brinza, L., & Benning, L. G. (2010). The determination of labile Fe in ferrihydrite by ascorbic acid extraction: Methodology, dissolution kinetics and loss of solubility with age and de-watering. *Chemical Geology*, *278*(1–2), 70–79. https://doi.org/10.1016/j.chemgeo.2010.09.002

Rapp, I., Schlosser, C., Browning, T. J., Wolf, F., Le Moigne, F. A. C., Gledhill, M., & Achterberg, E. P. (2020). El Nino-driven oxygenation impacts Peruvian shelf iron supply to the South Pacific Ocean. *Geophysical Research Letters*, *47*(7), e2019GL086631. https://doi.org/10.1029/2019GL086631

Resing, J. A., Sedwick, P. N., German, C. R., Jenkins, W. J., Moffett, J. W., Sohst, B. M., & Tagliabue, A. (2015). Basin-scale transport of hydrothermal dissolved metals across the South Pacific Ocean. *Nature*, *523*(7559), 200–U140. https://doi.org/10.1038/nature14577

Rijkenberg, M. J. A., Middag, R., Laan, P., Gerringa, L. J. A., Van Aken, H. M., Schoemann, V., et al. (2014). The distribution of dissolved iron in the West Atlantic Ocean. *PLoS One*, *9*(6), e101323. https://doi.org/10.1371/journal.pone.0101323

Rijkenberg, M. J. A., Powell, C. F., Dall'osto, M., Nielsdottir, M. C., Patey, M. D., Hill, P. G., et al. (2008). Changes in iron speciation following a Saharan dust event in the tropical North Atlantic Ocean. *Marine Chemistry*, *110*(1–2), 56–67. https://doi.org/10.1016/j.marchem.2008.02.006

Salt, L. A., Van Heuven, S. M. A. C., Claus, M. E., Jones, E. M., & De Baar, H. J. W. (2015). Rapid acidification of mode and intermediate waters in the southwestern Atlantic Ocean. *Biogeosciences*, *12*(5), 1387–1401. https://doi.org/10.5194/bg-12-1387-2015

Sarthou, G., Bucciarelli, E., Chever, F., Hansard, S. P., González-Dávila, M., Santana-Casiano, J. M., et al. (2011). Labile Fe(II) concentrations in the Atlantic sector of the Southern Ocean along a transect from the subtropical domain to the Weddell Sea Gyre. *Biogeosciences*, *8*(9), 2461–2479. https://doi.org/10.5194/bg-8-2461-2011

Schlitzer, R. (2023). Ocean data view. (Version 5.6.1) [Software]. odv.awi.de https://odv.awi.de/

Schlosser, C., Klar, J. K., Wake, B. D., Snow, J. T., Honey, D. J., Woodward, E. M. S., et al. (2014). Seasonal ITCZ migration dynamically controls the location of the (sub)tropical Atlantic biogeochemical divide. *Proceedings of the National Academy of Sciences of the United States of America*, *111*(4), 1438–1442. https://doi.org/10.1073/pnas.1318670111

Smith, R. M., Martell, A. E., & Motekaitis, R. J., & Standard Reference Data Program (National Institute of Standards and Technology). (2004). NIST critically selected stability constants of metal complexes database. (Version 8.0) [Dataset]. Standard Reference Data Program, National Institute of Standards and Technology, U.S. Department of Commerce. Retrieved from https://www.nist.gov/srd/nist46

Stockdale, A., Tipping, E., & Lofts, S. (2015). Dissolved trace metal speciation in estuarine and coastal waters: Comparison of WHAM/Model VII predictions with analytical results. *Environmental Toxicology & Chemistry*, *34*(1), 53–63. https://doi.org/10.1002/etc.2789

Stockdale, A., Tipping, E., Lofts, S., & Mortimer, R. J. G. (2016). Effect of ocean acidification on organic and inorganic speciation of trace metals. *Environmental Science & Technology*, *50*(4), 1906–1913. https://doi.org/10.1021/acs.est.5b05624

Tagliabue, A., Bowie, A. R., Boyd, P. W., Buck, K. N., Johnson, K. S., & Saito, M. A. (2017). The integral role of iron in ocean biogeochemistry. *Nature*, *543*(7643), 51–59. https://doi.org/10.1038/nature21058

Tagliabue, A., Bowie, A. R., DeVries, T., Ellwood, M. J., Landing, W. M., Milne, A., et al. (2019). The interplay between regeneration and scavenging fluxes drives ocean iron cycling. *Nature Communications*, *10*(1), 4960. https://doi.org/10.1038/s41467-019-12775-5

Tagliabue, A., Williams, R. G., Rogan, N., Achterberg, E. P., & Boyd, P. W. (2014). A ventilation-based framework to explain the regeneration-scavenging balance of iron in the ocean. *Geophysical Research Letters*, *41*(20), 7227–7236. https://doi.org/10.1002/2014GL061066

Takahashi, T., Sutherland, S. C., Chipman, D. W., Goddard, J. G., Ho, C., Newberger, T., et al. (2014). Climatological distributions of pH, pCO_2, total CO_2, alkalinity, and $CaCO_3$ saturation in the global surface ocean, and temporal changes at selected locations. *Marine Chemistry*, *164*, 95–125. https://doi.org/10.1016/j.marchem.2014.06.004

Tipping, E., Lofts, S., & Sonke, J. E. (2011). Humic ion-binding model VII: A revised parameterisation of cation-binding by humic substances. *Environmental Chemistry*, *8*(3), 225–235. https://doi.org/10.1071/En11016

Turner, D. R., Achterberg, E. P., Chen, C.-T. A., Clegg, S. L., Hatje, V., Maldonado, M. T., et al. (2016). Toward a quality-controlled and accessible Pitzer model for seawater and related systems. *Frontiers in Marine Science*, *3*. https://doi.org/10.3389/fmars.2016.00139

Uppström, L. R. (1974). The boron/chlorinity ratio of deep-sea water from the Pacific Ocean. *Deep-Sea Research and Oceanographic Abstracts*, *21*(2), 161–162. https://doi.org/10.1016/0011-7471(74)90074-6

Voelker, C., & Tagliabue, A. (2015). Modeling organic iron-binding ligands in a three-dimensional biogeochemical ocean model. *Marine Chemistry*, *173*, 67–77. https://doi.org/10.1016/j.marchem.2014.11.008

Ye, Y., Völker, C., & Gledhill, M. (2020). Exploring the iron-binding potential of the ocean using a combined pH and DOC parameterization. *Global Biogeochemical Cycles*, *34*(6). https://doi.org/10.1029/2019GB006425

Zark, M., & Dittmar, T. (2018). Universal molecular structures in natural dissolved organic matter. *Nature Communications*, *9*(1), 3178. https://doi.org/10.1038/s41467-018-05665-9

Zhang, J., Kattner, G., & Koch, B. P. (2019). Interactions of trace elements and organic ligands in seawater and implications for quantifying biogeochemical dynamics: A review. *Earth-Science Reviews*, *192*, 631–649. https://doi.org/10.1016/j.earscirev.2019.03.007

Zhu, K., Birchill, A. J., Milne, A., Ussher, S., Humphreys, M. P., Carr, N., et al. (2021). Equilibrium calculations of iron speciation and apparent iron solubility in the Celtic Sea at ambient seawater pH using the NICA-Donnan model. *Marine Chemistry*, *237*, 104038. https://doi.org/10.1016/j.marchem.2021.104038

Zhu, K., Groenenberg, J. E., Achterberg, E. P., & Gledhill, M. (2022). Modelling protocols for derivation of Fe(III) NICA constants and calculations of ambient Fe speciation and apparent Fe(III) solubility in seawater [Software]. https://doi.org/10.17504/protocols.io.brc4m2yw

Zhu, K., Hopwood, M. J., Groenenberg, J. E., Engel, A., Achterberg, E. P., & Gledhill, M. (2021). Influence of pH and dissolved organic matter on iron speciation and apparent iron solubility in the Peruvian shelf and slope region. *Environmental Science & Technology*, *55*(13), 9372–9383. https://doi.org/10.1021/acs.est.1c02477

References From the Supporting Information

Milne, C. J., Kinniburgh, D. G., & Tipping, E. (2001). Generic NICA-Donnan model parameters for proton binding by humic substances. *Environmental Science & Technology*, *35*(10), 2049–2059. https://doi.org/10.1021/es000123j